Energy 250 (2022) 123827

Contents lists available at ScienceDirect

Energy

journal homepage: www.elsevier.com/locate/energy

Air-breathing versus conventional polymer electrolyte fuel cells: A parametric numerical study

Fatma Calili-Cankir [a, b], Mohammed S. Ismail [a, c, *], Derek B. Ingham [a], Kevin J. Hughes [a], Lin Ma [a], Mohamed Pourkashanian [a, c]

[a] Energy 2050, Department of Mechanical Engineering, Faculty of Engineering, University of Sheffield, Sheffield, S3 7RD, United Kingdom
[b] Department of Energy Systems Engineering, Iskenderun Technical University, Hatay, 31 200, Turkey
[c] Translational Energy Research Centre, University of Sheffield, Sheffield, S9 1ZA, United Kingdom

ARTICLE INFO

Article history:
Received 20 August 2021
Received in revised form
10 March 2022
Accepted 25 March 2022
Available online 28 March 2022

Keywords:
Air-breathing PEFCs
Conventional PEFCs
Natural convection
Forced convection
Heat and mass transfer

ABSTRACT

Two mathematical models have been built for air-breathing and conventional polymer electrolyte fuel cells to explore the reasons affecting the cell performance. A parametric study has been conducted to (i) investigate how each type of fuel cells responds to changes in some key parameters and (ii) consequently obtain some insights on how to improve the performance of the air-breathing fuel cell. The conventional fuel cell significantly outperforms the air-breathing fuel cell and this is due to substantially higher forced convection-related heat and mass transfer coefficients associated with the conventional fuel cell as compared with natural convection-related heat and mass transfer coefficients associated with air-breathing fuel cell. The two types of fuel cell respond differently to changes in porosity and thickness of gas diffusion layer: the conventional fuel cell performs better with increasing porosity of gas diffusion layer (from 0.4 to 0.8) and decreasing thickness of gas diffusion layer (from 700 to 100 μm) while the air-breathing fuel cell performs better with decreasing porosity and increasing thickness of gas diffusion layer. Further, the air-breathing fuel cell was found to be more sensitive to membrane thickness and less sensitive to electrical resistance compared to conventional fuel cell.

1. Introduction

There is an increasingly urgent need to convert to renewable energy sources in order to avoid the detrimental consequences of climate change phenomena [1–3]. In this regard, polymer electrolyte fuel cells (PEFCs) are promising zero-emission power conversion technologies which form a central pillar in hydrogen economy and this is due their high efficiency, low operating temperature and rapid start-up [4,5]. In conventional PEFCs, the reactants (hydrogen and oxygen), and products (water vapour) are transported from/to the flow channels to/from the membrane electrode assembly (MEA) of the fuel cell by mainly forced convection using auxiliary components such as compressors and flow controllers. Further, the reactant gasses are normally required to be humidified by an external humidifier before entering the fuel cell to ensure appropriate initial membrane hydration and subsequently reasonably good ionic conductivity [6–8]. These auxiliary components (e.g., the compressors and humidifiers) substantially increase the overall size and the weight and subsequently the cost and complexity of the fuel cell system. On the other hand, small electronic devices (e.g., smartphones and tablets) have become increasingly essential in our daily life and they consequently form a huge market [9]. The powering components of these devices should be ideally very small to ease carrying and handling. Therefore, the conventional PEFC system should be substantially simplified to reduce its size and weight if it is to compete with the commonly-used rechargeable batteries. To this end, air-breathing PEFC technology has been proposed.

In air-breathing PEFCs, the cathode side of the fuel cell is open to the ambient and this allows for the oxidant (air) and humidifying water to be directly extracted from the ambient by natural convection, thus eliminating the need to have an oxygen storage device, a mass flow controller, a humidifier, and a pumping device. However, natural convection-related heat and mass transfer coefficients are significantly smaller than those of forced convection, imposing increased heat and mass transfer resistance for air-

* Corresponding author. Translational Energy Research Centre, University of Sheffield, Sheffield, S9 1ZA, United Kingdom.
E-mail address: m.s.ismail@sheffield.ac.uk (M.S. Ismail).

https://doi.org/10.1016/j.energy.2022.123827

breathing PEFCs and significantly limiting the cell performance when compared with conventional PEFCs. Mathematical modelling is one of the most efficient and cost-effective ways to better understand the physics within the fuel cells and/or look into ways (either design-wise or material-wise) to improve their performance. There have been numerous models in the literature for the conventional PEFCs; see for example [10–16]. On the other hand, the number of air-breathing PEFC numerical models is scarce and this is clearly due to the limited number of applications in which this technology is used. In the following paragraphs, we summarise the key findings of the mathematical models for the air-breathing fuel cells that were encountered while performing the literature review.

Zhang and Pitchumani [17] built a two-dimensional and non-isothermal model for an air-breathing PEFC with a dual-cell hydrogen cartridge to investigate the effects of cell geometry and operating conditions on the performance of the fuel cell. They found that the performance of the fuel cell is improved by reducing the side length of the fuel cell and this is due to better the exposure to ambient air, thus enhancing the utilisation of the active area. They also found that the fuel cell performs better with increasing the anode pressure and relative humidity. In another study performed by the same research group, Zhang et al. [18] developed a three-dimensional and non-isothermal mathematical model to investigate the effect of geometrical parameters of an air-breathing PEFC stack, consisting of two cells sharing a hydrogen chamber. They concluded that the vertical gap between the fuel cell and the substrate requires to be minimum in order to improve the supply of air to the cathode catalyst layers and, therefore, improve the cell performance.

O'Hayre et al. [19] developed a one-dimensional and non-isothermal model for an air-breathing PEFC and they found that the fuel cell behaviour is adversely and significantly influenced by the fact that the boundary layer of natural convection is the main barrier that restricts heat and mass transfer to the open cathode of the fuel cell. They also showed that the cell performance is strongly affected by even slight forced convection. Litster et al. [20] proposed a two-dimensional numerical model for an air-breathing PEFC with a nano-porous gas diffusion layer (GDL). They showed that air is mainly transported by Knudsen diffusion in the proposed GDL, which provides sufficient amount of oxygen to the active side of the cathode catalyst layer. Calili et al. [21] built a dynamic model for an air-breathing PEFC and investigated the effects of ambient conditions and GDL parameters (i.e. the GDL thickness and thermal conductivity) on the dynamic response of the fuel cell during load changes. They found that there exist an optimum ambient temperature (20 °C) and GDL thickness (i.e. 500 μm) at which the fuel cell shows better steady-state performance and less overshoots in the voltage during the load changes. They also found that the thermal conductivity of the GDL needs to be reasonably high in order to improve the performance and load following ability of the fuel cell. Rajani and Kolar [22] developed a two-dimensional model for an air-breathing PEFC and investigated the effect of ambient conditions (20–80% relative humidity and 10–40 °C) on the performance of the fuel cell. They reported that the ambient temperature predominantly influences the performance of the fuel cell compared to the ambient relative humidity. Chen et al. [23] proposed a mathematical model in order to investigate the effect of hydrogen relative humidity on the performance of air-breathing PEFCs at different ambient temperatures (10, 20 and 30 °C). They found that the hydrogen relative humidity significantly influences the performance of the fuel cell; for example, the limiting current density could increase by more than 40% when the hydrogen relative humidity increases from 0% to 100% at an ambient temperature of 30 °C. Matamoros and Brüggemann [24] created a three-dimensional model for an air-breathing PEFC and investigated the effects of the ambient conditions on the concentration and ohmic losses. They found that the performance of the fuel cell improves with increasing ambient temperature due to the fact that the increase in the temperature gradient enhances natural convection. They also demonstrated that mass transport losses dominantly influence the performance of the fuel cell compared to ohmic losses at different ambient conditions.

Ying et al. [25] built a two-dimensional model for a channel-based air-breathing PEFC. They found that there exists an optimum opening ratio for the open cathode at which the fuel cell performance is maximized. In their subsequent works, they developed three-dimensional and non-isothermal models for air-breathing PEFCs to investigate: (i) the temperature distribution and cell performance [26], (ii) the effects of the channel configuration [27] and (iii) interactions between electrochemical reactions, heat and mass transfer in the fuel cell [28]. Hwang [29] created a three-dimensional model for an air-breathing PEFC with an array of circular holes at the cathode current collector. They suggested that the fuel cell with the staggered arrangement for holes shows slightly better performance than that with the in-line arrangement for the holes. They also found that the optimum opening ratio for both arrangements is about 30%, which provides a balance between the mass transport losses and the ohmic losses. A two-dimensional model for an air-breathing PEFC with rectangular vertical opening at the cathode current collector was developed by Schmitz et al. [30]. Their results showed that the cell performance enhances when the opening ratio of the current collector increases from 33 to 80%.

Kumar and Kolar [31] developed a three-dimensional and non-isothermal model for an air-breathing PEFC and investigated the effects of cathode collector type (channel- and window-based) on the fuel cell performance. They showed that the fuel cell performs better with window-based cathode current collector than with the channel based current collectors due to the fact that the rate of transport rate of the produced water and heat is higher in the fuel cell equipped with the former current collector type.

A three-dimensional mathematical model for a commercial air-breathing PEFC was developed by Henriques et al. [32]. The model was used to predict the performance of the fuel cell when the transversal channels (barriers in the channels to increase contact resistance) in the original design of the fuel cell is eliminated. The redesigned fuel cell was fabricated and experimentally tested. They validated the model with the experimental data and concluded that the efficiency of the fuel cell improved by about 26% after redesigning.

Ismail et al. [33] built a two-dimensional thermal model for an air-breathing PEFC. They showed that the Joule heating has a significant impact on the modelled thermal parameters. They also demonstrated that although the effect of entropic heat is not as significant as the Joule heating, it cannot be ignored at low current densities. Later, they [34] developed a non-isothermal mathematical model under steady-state conditions to investigate the impacts of heat sources on the performance of air-breathing PEFCs. They found that the fuel cell performance is significantly over-predicted if the entropic heat and/or Joule heat are neglected.

Recently, Yan et al. [35] performed a numerical simulation for an air-breathing PEFC stack applying different cathode flow channel designs in order to enhance the performance of the fuel cell. The numerical results were validated by experimental data and showed that the optimum opening ratio is between 50 and 60% shows a better performance due to reduced and uniform stack temperature. Lee et al. [36] developed a three-dimensional, two-phase and multiscale model for an air-breathing PEFC to parametrically investigate the transport of water and heat. They found that the

performance of the fuel cell improves with the use of a thinner membrane and higher ionomer fraction in the cathode catalyst layer due to reduced ionic resistance of the membrane phase. Al-Anazi et al. [37] performed a computational investigation using a three-dimensional, non-isothermal, steady-state model for an air-breathing PEFC stack to investigate the effect of ambient conditions in Riyadh City (Saudi Arabia) on the performance of the fuel cell. They found that the fuel cell stack performs better with warm and humid ambient conditions (summer time) where the humidification of the membrane is adequately maintained. On the other hand, the performance of fuel cell stack during the winter time was found to be around 12% less than that in summer time. Lee et al. [38] built a three-dimensional air-breathing PEFC model incorporating an innovative cathode flow-field design. They found that the proposed cathode flow-field configuration increases the water-retaining capability of the fuel cell by around 10% compared to that of the conventional cathode flow-field configuration where the channels are parallel.

To the best of the authors' knowledge, there have been no modelling studies in the literature that simultaneously compared and analysed the outcomes of the air-breathing and the conventional PEFCs. To this end, two steady-state, non-isothermal and efficient mathematical models have been developed for both conventional and air-breathing PEFCs to conduct for the first time a parametric study to (i) explore the parameters that impact each type of fuel cells and subsequently (ii) obtain insights on how to improve the air-breathing fuel cell performance. To achieve this goal, the sensitivity analysis of both modelled fuel cells to some key parameters (i.e. the porosity and the thickness of the GDL, the membrane thickness and the overall electrical resistance) has been performed. These parameters have been selected because they could be practically changed in order to improve the performance of the fuel cells. Namely, the porosity and the thickness of the GDL could be easily adapted by employing different types of GDLs or refining the existing GDLs. This note also applies to the thickness of the membrane electrolyte which is the only parameter that could be changed assuming using the conventionally-used Nafion® membranes. The overall electrical resistance is mainly due to contact resistance between the various components of the fuel cells and could be controlled through varying the assembling compression. The parametric study has not included in the impact of the operating conditions (the temperature and relative humidity) as these parameters are dictated by those of the ambient adjacent to the open cathode of the air-breathing PEFCs; this is not the case for the conventional PEFC where the operating conditions could be controlled. Therefore, commonly-encountered ambient conditions (20 °C and 40% relative humidity) where fixed and used for both air-breathing and conventional PEFCs. It should be noted we have investigated the impact of the ambient conditions on the performance of air-breathing PEFCs in a previous work [21]. It is noteworthy that the model has been originally developed for the air-breathing PEFC [34]. However, some improvements and adaptations to the model have been made. Namely, the membrane electrolyte and the anode compartment have been included into the model and, consequently, the relevant physics (the heat transport in the anode GDL and the electrolyte, the transport of gases in the anode and the transport of dissolved water through the membrane) have been accounted for. Further, for the purpose of this comparative study, the physics of the model have been adapted to represent the corresponding conventional PEFC.

2. Model formulation

Most of the equations listed in this section are applicable for both types of fuel cells: conventional and air-breathing PEFCs. The modelled air-breathing PEFC was originally reported by Fabian et al. [39]. The cell geometry and MEA properties of the modelled conventional PEFC have been set to be the same as those of the air-breathing PEFC described by Fabian et al. [39]. The following assumptions and considerations have been employed for the models:

(i) The fuel cells operate under steady state conditions.
(ii) Water exists only in vapour form.
(iii) The reactant gases are treated as ideal gases.
(iv) The anode of the air-breathing PEFC is in dead-end mode.
(v) The main mode of transport in GDLs is diffusion and therefore the contribution of the convective flow in GDLs is negligible.
(vi) The cathode catalyst layer is infinitely thin so that it is treated as an interface between the membrane and the GDLs.
(vii) The water activity is in equilibrium with water vapour activity in the catalyst layers.
(viii) The concentration losses are neglected as the water activity has been always less than unity and the amount of reactants available for the reactions have been always sufficient for all the investigated cases.
(ix) The only heat source occurs at the cathode catalyst layer and all the other heat sources are neglected due to their small amounts.

Fig. 1 shows the schematics of the modelled cells displaying the key components and the heat and mass fluxes for each fuel cell type.

Note that Fabian et al. [39] reported that some water accumulates at the cathode of the air-breathing PEFC, particularly at the intermediate current densities for low temperatures and high humidity conditions. However, accumulation of liquid water starts to diminish as the current density increases since the running air-breathing fuel cell was of high-performance. This is due to the exponential increase in the cell temperature at high current densities. The sharp decline in the cell potential at high current densities is, therefore, primarily due to membrane dehydration, not water flooding. Therefore (considering that water flooding may only occur in the intermediate current densities of the modelled fuel cell and this does not change the overall trends of the outcomes of the models), water is, for simplification, assumed to exist in water vapour form only [21]. This assumption/simplification was also considered by O'Hayre et al. [19] and Ismail et al. [34].

2.1. Cell voltage

The cell voltage, V_{cell}, is calculated as follows:

$$V_{cell} = E - \eta_{act} - \eta_{ohmic} \tag{1}$$

where E is the reversible (or Nernst) voltage, η_{act} is the activation losses and η_{ohmic} is the ohmic losses. The reversible voltage is obtained using the Nernst equation [40]:

$$E = \frac{-\Delta H + T\Delta S}{2F} + \frac{RT}{2F}\ln\left(\frac{P_{H_2}.P_{O_2}^{1/2}}{P_{H_2O}}\right) \tag{2}$$

where P_{H_2}, P_{O_2} and P_{H_2O} are the partial pressures of hydrogen, oxygen and water under equilibrium conditions, respectively. T is the absolute temperature, R is the universal gas constant and F is the Faraday's constant. ΔH and ΔS are the enthalpy and entropy changes for the overall reaction, respectively. The activation losses are obtained using the following expression [19,40]:

$$\eta_{act} = \frac{RT}{2\alpha F} \ln\left(\frac{C_{O_2}^{\infty/ch} j}{C_{O_2}^{ccl} j_0}\right) \tag{3}$$

where $C_{O_2}^{\infty/\mathrm{ch}}$ and $C_{O_2}^{ccl}$ are the molar concentrations of oxygen at the ambient/flow channel and the cathode catalyst layer, respectively. α is the charge transfer coefficient, j is the current density and j_0 is the reference exchange current density, corrected for temperature by the following expression:

$$j_0 = j_{298\ K}^0 \exp\left[\frac{E_a}{R}\left(\frac{1}{298} - \frac{1}{T}\right)\right] \tag{4}$$

where E_a is the activation energy. The ohmic losses can be expressed as follows [19,21,34]:

$$\eta_{ohmic} = jA_{act}(R_{elec} + R_{mem}) \tag{5}$$

where A_{act} represents the active area of the fuel cell, R_{elec} and R_{mem} are respectively the lumped electrical resistance of the cell and the membrane resistance. R_{mem} is given by:

$$R_{mem} = \frac{\delta_{mem}}{A_{act}\sigma_{mem}} \tag{6}$$

where δ_{mem} is the thickness of the Nafion® membrane. The ionic conductivity of the membrane, σ_{mem} can be calculated using the following empirical correlation for the air-breathing PEFC [41]:

$$\sigma_{mem} = \left(3.46a^3 + 0.0161a^2 + 1.45a - 0.175\right)\exp\left[1268\left(\frac{1}{303} - \frac{1}{T}\right)\right] \tag{7}$$

and using the well-known Springer's model for the conventional PEFCs [42,43]:

$$\sigma_{mem} = [0.514\lambda - 0.326]\exp\left[1268\left(\frac{1}{303} - \frac{1}{T}\right)\right] \tag{8}$$

where λ represents the water content of the membrane and is given by Ref. [44]:

$$\lambda = \begin{cases} 0.043 + 17.81a - 39.85a^2 + 36a^3, & 0 < a \le 1 \\ 14 + 1.4(a-1), & 1 < a \le 3 \end{cases} \tag{9}$$

The water activity, a is defined as follows [40]:

$$a = \frac{P_{H_2O}}{P_{sat}} \tag{10}$$

where P_{H_2O} and P_{sat} represent the partial pressure and the saturation pressure of water vapour at the catalyst layers, respectively. P_{sat}, in *atm*, is given by Refs. [42,45]:

$$\log_{10} P_{sat} = -2.1794 + 0.02953(T - 273.15) - 9.1837 \times 10^{-5}(T - 273.15)^2 + 1.4454 \times 10^{-7}(T - 273.15)^3 \tag{11}$$

It should be noted that the water activity has been limited to one when calculating the ionic conductivity of the membrane in the modelled air-breathing PEFC; water activity beyond unity results in unrealistic values for the ionic conductivity of the membrane [19,34].

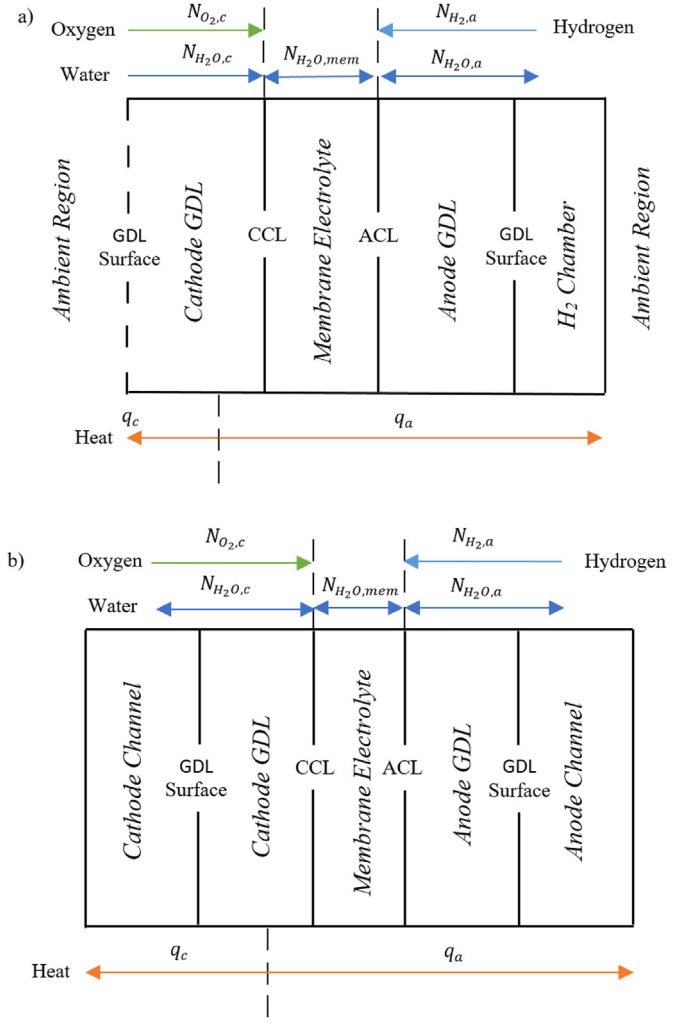

Fig. 1. Schematic representations of the modelled: (a) air-breathing and (b) conventional PEFCs. Note that the symbol 'N' stands for molar flux, 'q' for heat flux, 'CCL' for cathode catalyst layer and 'ACL' for anode catalyst layer, the subscript 'a' for anode and the subscript 'c' for cathode.

2.2. Heat transfer

Heat is mainly produced at the cathode catalyst layer as a result of the exothermic oxygen reduction reaction, thus creating a temperature difference between the cathode catalyst layer and the two outermost sides of the fuel cells. The generated heat is first conducted through the solid-phase of the fuel cell components (i.e. the GDLs, the membrane and the current collectors) and is then transported at the interfaces with the ambient through convection. As schematically illustrated in Fig. 1, the temperature gradients are created between the cathode catalyst layer interface (where most of the heat sources exist) and the ambient regions at both sides of

the fuel cell. The heat generated in the fuel cell is mathematically given as [34]:

$$q = q_c + q_a = j\left(\eta_{act} + \eta_{ohm} + \frac{T\Delta S}{2F}\right) \tag{12}$$

The left-hand side heat flux, q_c (see Fig. 1), may be expressed as follows:

$$q_c = \begin{cases} k_{GDL}\dfrac{T_{ccl} - T_{gdl,c}}{\delta_{gdl,c}} = h\left(T_{gdl,c} - T_\infty\right) \text{ for air} - \text{breathing PEFC} \\ k_{GDL}\dfrac{T_{ccl} - T_{gdl,c}}{\delta_{gdl,c}} = h\left(T_{gdl,c} - T_{cell}\right) \text{ for conventional PEFC} \end{cases} \tag{13}$$

and the right-hand side heat flux, q_a (see Fig. 1), may be given by:

$$q_a = \begin{cases} \dfrac{T_{ccl} - T_{gdl,a}}{\left(\dfrac{\delta_{mem}}{k_{mem}} + \dfrac{\delta_{gdl,a}}{k_{gdl}}\right)} = h\left(T_{gdl,a} - T_\infty\right) \text{ for air} - \text{breathing PEFC} \\ \dfrac{T_{ccl} - T_{gdl,a}}{\left(\dfrac{\delta_{mem}}{k_{mem}} + \dfrac{\delta_{gdl,a}}{k_{gdl}}\right)} = h\left(T_{gdl,a} - T_{cell}\right) \text{ for conventional PEFC} \end{cases} \tag{14}$$

where T_∞, T_{cell}, T_{ccl}, $T_{gdl,c}$ and $T_{gdl,a}$ respectively represent the ambient temperature, the cell temperature (which is equivalent to the temperature of the gases flowing in the channel) and the temperatures at the cathode catalyst layer, at the cathode GDL surface and at the anode GDL surface. The cathode GDL, the anode GDL and the membrane thickness are designated as $\delta_{gdl,c}$, $\delta_{gdl,a}$ and δ_{mem}, respectively. k_{gdl} and k_{mem} are the thermal conductivities of the GDL and the membrane, respectively.

h is the heat transfer coefficients the fuel cell has with the ambient or the flow channel. h for either side of the air-breathing PEFCs is the sum of the radiative heat transfer coefficient h_{rad} and the convective heat transfer coefficient h_{conv} [46]:

$$h_{rad} = 2e\sigma_{Bolt}\left(T_{gdl}^2 + T_\infty^2\right)\left(T_{gdl} + T_\infty\right) \tag{15}$$

$$h_{conv} = \frac{Nu.k_{air}}{L_{ch}} \tag{16}$$

where e and σ_{Bolt} are the emissivity and the Stephan-Boltzmann constant, respectively. k_{air} is the thermal conductivity of air and L_{ch} is the characteristic length for heat transfer which is, for the air-breathing fuel cell, equal to 7 cm. Nu is the Nusselt number which is obtained for a horizontally-oriented iso-flux heated plate (representing the air-breathing PEFC modelled in this work) using the following expressions [46,47]:

$$Nu_c = 0.16Ra_c^{1/3} \tag{17}$$

$$Ra = \frac{g\beta q L_{ch}^4}{\nu_{air}\alpha_{air}k_{air}} \tag{18}$$

where Ra is the Rayleigh number. ν_{air} and α_{air} are the kinematic viscosity and the thermal diffusivity of air, respectively. All the thermo-physical properties of air used in the equations have been estimated using the tabulated data in Ref. [46] at the film temperature. The film temperature at the interface between the ambient and the cathode GDL, T_f, is defined as the arithmetic mean of the temperature of the cathode GDL surface, T_{gdl}, and the ambient temperature, T_∞. The thermal expansion coefficient at the interface, β is estimated as follows [21]:

$$\beta = {}^1\!/_{T_f} \tag{19}$$

On the other hand, h for the conventional fuel cell is represented by only the convective heat transfer coefficient and this is (as evidenced from not shown simulations) due to negligible dissipation of heat through radiation [46]:

$$h_{conv} = \frac{Nu.k_i}{L_{ch}} \tag{20}$$

where k_i is the thermal conductivity of the species i (air in the cathode flow channel and hydrogen in the anode flow channel). The characteristic length L_{ch} is the hydraulic diameter of the channel which is in this case the side length of the square cross-section (i.e., 1 mm). The Nusselt number for an iso-flux fully developed laminar flow in a rectangular channel is given by Ref. [46]:

$$Nu = 3.61 \tag{21}$$

2.3. Mass transfer

Oxygen and water are transported by natural convection between the ambient and the cathode GDL in the air-breathing PEFC. On the other hand, oxygen, hydrogen and water vapour are transported by forced convection between the flow channel and the cathode/anode GDL of the conventional PEFC. The anode of the air-breathing PEFC is dead-ended and therefore, the concentration of dry hydrogen at the surface of the anode GDL is assumed to be that of the hydrogen chamber (see Fig. 1). All the gases in both types of the fuel cells are mainly transported by diffusion within the GDLs. The driving force for the transport of the gases between the ambient/channel and the catalyst layer is the consumption/generation of these gases at the catalyst layers. All the above description could be mathematically described as follows:

$$N_i = \frac{j}{nF} = D_{ij}^{eff}\frac{C_i^{gdl} - C_i^{cl}}{\delta_{gdl}} = h_{m,i}\left(C_i^{gdl} - C_i^{\infty/ch}\right) \tag{22}$$

The second term in the above equation is the Faraday's second low of electrolysis. N_i is the molar flux of the species i (oxygen, hydrogen or water vapour), j is the current density of the fuel cell, n is the number of electrons transferred per 1 mol of oxygen (4), water (2) or hydrogen (2). C_i^{gdl}, C_i^{cl} and $C_i^{\infty/ch}$ are respectively the molar concentration of the species i at the GDL surface, at the catalyst layer and in the ambient/flow channel and C_i^{cl} is the molar concentration of the species i in the catalyst layer. The effective diffusion coefficient on the cathode side, D_{ij}^{eff} is effective diffusion coefficient of the species i into j (oxygen and water vapour into air in the cathode GDL or hydrogen into water vapour in the anode GDL) and is estimated using the following expression [48]:

$$D_{ij}^{eff} = f(\varepsilon).D_{ij}\left(\frac{T_{gdl}}{T_{ref}}\right)^{1.5}\left(\frac{P_{ref}}{P}\right) \tag{23}$$

where D_{ij} is the binary diffusion coefficient of the species i into j at the reference temperature (T_{ref}) and pressure (P_{ref}). Both the

operational pressure (P) and the reference pressure are equal to the ambient pressure, i.e. 1 atm, and therefore the last term in Eq. (23) is unity. Note that T_{gdl} in Eq. (23) is taken to be the arithmetic mean of the surface temperature of the GDL and the temperature at the catalyst layer. The diffusibility, $f(\varepsilon)$, is a function of the porosity of the GDL and is calculated using the following empirical correlation [49]:

$$f(\varepsilon) = 1 - 2.72\varepsilon \cosh(2.53\varepsilon - 1.61)\left(\frac{3(1-\varepsilon)}{3-\varepsilon}\right) \tag{24}$$

The mass transfer coefficient of the species i ($h_{m,i}$) is estimated as follows:

$$h_{m,i} = \frac{Sh_i.D_{ij}}{L_{ch,m}} \tag{25}$$

where $L_{ch,m}$ is the characteristic length related to the mass transfer (which is equal to the side length of the square channel for the conventional fuel cell (1 mm) and equal to the side length of active area for the air-breathing fuel cell (3 cm)). Sh is Sherwood number and is, making use of the analogy between heat transfer and mass transfer, given as [46,47]:

$$Sh_i = \begin{cases} 3.61 \quad for\ conventional\ PEFC \\ 0.16Ra_{m,i}^{1/3}\ for\ air-breathing\ PEFC \end{cases} \tag{26}$$

$Ra_{m,i}$ is the Rayleigh number associated with the mass transfer for the species i and can be calculated using the following expression [47]:

$$Ra_{m,i} = \frac{g\gamma(x_i^{\infty} - x_i)L_{ch,m}^3}{\nu_i D_{ij}} \tag{27}$$

where g is the acceleration due to gravity, x_i^{∞} is the mole fraction of the species$i$ in the ambient region, x_i is the mole fraction of the species i at the surface of the GDL and ν_i is the kinematic viscosity of the species i. Due to the fact that the nitrogen concentration within the cell and the ambient region remains almost constant, a binary mixture of ideal gases of oxygen and water vapour can be assumed; therefore, the volumetric expansion coefficient of species i due to the concentration gradients, γ, is estimated as follows [47]:

$$\gamma = \frac{M_{O_2} - M_{H_2O}}{M_{mix}} \tag{28}$$

where M_{O_2} and M_{H_2O} are the molecular weights of oxygen and water, respectively. The molecular weight of the binary mixture, M_{mix}, has been taken to be the arithmetic mean of the molecular weights of the binary mixture in the ambient region, M_{mix}^{∞}, and at the GDL surface, M_{mix}^{gdl} [34]:

$$M_{mix} = \frac{M_{mix}^{\infty} + M_{mix}^{\mathrm{gdl}}}{2} \tag{29}$$

where M_{mix}^{∞} is given by:

$$M_{mix}^{\infty} = \frac{C_{O_2}^{\infty}}{C_{O_2}^{\infty} + C_{H_2O}^{\infty}} M_{O_2} + \frac{C_{H_2O}^{\infty}}{C_{O_2}^{\infty} + C_{H_2O}^{\infty}} M_{H_2O} \tag{30}$$

$C_{O_2}^{\infty}$ is the molar concentration of oxygen in the ambient region:

$$C_{O_2}^{\infty} = 0.21\left(C_{tot}^{\infty} - C_{H_2O}^{\infty}\right) \tag{31}$$

The molar concentration of water in the ambient air, $C_{H_2O}^{\infty}$ is given by:

$$C_{H_2O}^{\infty} = \frac{P_{sat}^{\infty}.RH}{RT_{\infty}} \tag{32}$$

where RH represents the water relative humidity of the ambient. The water vapour saturation pressure P_{sat}^{∞} is obtained using Eq. (11).

The molar concentration of ambient air C_{tot}^{∞} is obtained using the ideal gas law:

$$C_{tot}^{\infty} = \frac{P}{RT_{\infty}} \tag{33}$$

In a similar way, M_{mix}^{gdl} is calculated using Eq. (30) by replacing the molar concentrations of oxygen and water in the ambient with those at the surface of the cathode GDL.

It should be noted that the membrane electrolyte is impermeable to oxygen, hydrogen and nitrogen but allows for water (in dissolved form) to transport within it by electro-osmotic drag (driven by the proton transport and is from the anode side to cathode side of the membrane) and back diffusion which is normally from the cathode side to anode side. To this end, the molar flux of water N_{H_2O} at either the cathode or the anode catalyst layer (calculated using Eq. (22)) is equal to the net water flux resulting as a result of the competing transport phenomena of electro-osmotic drag and back diffusion [50]:

$$N_{H_2O} = \begin{cases} n_d\frac{j}{F} - D_w\frac{C_{H_2O}^{ccl} - C_{H_2O}^{acl}}{\delta_{mem}}\ at\ the\ cathode\ catalyst\ layer \\ D_w\frac{C_{H_2O}^{ccl} - C_{H_2O}^{acl}}{\delta_{mem}} - n_d\frac{j}{F}\ at\ the\ anode\ catalyst\ layer \end{cases} \tag{34}$$

where $C_{H_2O}^{ccl}$ and $C_{H_2O}^{acl}$ are the molar concentrations of water at the cathode and the anode catalyst layers respectively. D_w is the dissolved water diffusivity in the membrane and n_d is the electro-osmotic drag coefficient. These two parameters are given as follows [50]:

$$D_w = \begin{cases} 3.1\times10^{-7}\lambda(\exp(0.28\lambda) - 1)\exp\left(-\frac{2346}{T}\right) \quad for\ 0 < \lambda < 3 \\ 4.17\times10^{-8}\lambda(161\exp(-\lambda) + 1)\exp\left(-\frac{2346}{T}\right)\ for\ \lambda \geq 3 \end{cases} \tag{35}$$

and

$$n_d = \begin{cases} 1 \quad for\ \lambda \leq 14 \\ 0.1875\lambda - 1.625 \quad for\ \lambda > 14 \end{cases} \tag{36}$$

The water content of the membrane, λ, is calculated using Eqs. (8)–(10). It should be noted that the water diffusivity and the electro-osmotic drag coefficient have been taken to be the arithmetic mean of their values at the temperatures of the anode and cathode catalyst layers.

2.4. Numerical procedure

The computational domain of each fuel cell consists of a cathode GDL, cathode catalyst layer, membrane electrolyte, anode catalyst layer and anode GDL (Fig. 3). The boundary layers next to the cathode of air-breathing PEFC are induced by natural convection and are for temperature and concentrations. The initial cell

Table 1
Physical parameters and constants used for the base cases of the models [19,34,39].

Parameters	Value
Universal gas constant, R	8.314 J/(mol.K)
Faraday's constant, F	96,485 C/mol
Stephan-Boltzmann constant, σ_{Bolt}	5.67×10^{-8} W/(m^2.K^4)
Gravitational acceleration, g	9.81 m/s^2
Ambient/cell pressure, P	1 atm
Oxygen/nitrogen molar ratio	21/79
Ambient temperature, T_∞	20 °C
Initial cell temperature of conventional PEFC, T	20 °C
Binary diffusivity of O_2 in air, $D_{O_2,air}$	2.20×10^{-5} m^2/s
Binary diffusivity of H_2O in air, $D_{H_2O,air}$	2.56×10^{-5} m^2/s
Binary diffusivity of H_2 into water vapour, D_{H_2}	2.59×10^{-10} m^2/s [17]
Cell active area, A_{act}	9.00×10^{-3} m^2
Membrane thickness, δ_{mem}	5.20×10^{-5} m
GDL thickness, δ_{gdl}	3.00×10^{-4} m
GDL porosity, ε	0.70
GDL tortuosity, τ	3
GDL thermal conductivity, k_{gdl}	1 W/(m.K)
Membrane thermal conductivity, k_{mem}	0.17 W/(m.K)
Emissivity, e	0.90
Reference exchange current density, j^0_{298K}	3 mA/cm^2
Lumped cell electrical resistance, R_{elec}	12 mΩ
Charge transfer coefficient, α	0.41
Enthalpy change, ΔH	-241.98×10^3 J/mol
Entropy change, ΔS	-44.43×10^3 J/mol
Activation energy, E_a	50.00×10^3 J/mol

temperature of the conventional PEFC has been set to be the same with the ambient temperature. Table 1 shows the physical parameters used for the modelled of the air-breathing and conventional fuel cells; except for the characteristic lengths, the parameters for both models have been kept the same for comparative purposes. All the physical parameters and constants of the fuel cells have been declared for each model and all the equations mentioned in Section 2.1, 2.2 and 2.3 have been appropriately listed in an m-file within MATLAB®. Eqs ((1) and (12)–(14) and (22) and (34) have been then solved for current density, concentrations and temperatures at different cell potentials and interfaces using the nonlinear solver 'fsolve'.

3. Results and discussion

Fig. 2(a-b) shows that the polarisation curve and the surface temperature of the cathode GDL of the modelled air-breathing PEFC at ambient temperature and relative humidity of 20 °C and 40% are in very good agreement with the corresponding experimental data reported in Ref. [39]. Further, the model nicely captures the experimentally observed sharp decline in the cell performance (Fig. 2a) and exponential increase in the cell temperature (Fig. 2b) at high current densities. The graphs in Fig. 2(a-b) also present the data generated by the modelled conventional PEFC at 20 °C cell temperature and 40% relative humidity of inlet gases. It is clear from Fig. 2a that the conventional PEFC significantly outperforms the air-breathing PEFC as primarily evidenced by the decreased limiting current density demonstrated by the latter fuel cell. Some more data have been generated from both models and plotted in order to highlight the underlying reasons behind the above performance difference between the two types of fuel cells; see Fig. 2(c-f).

Both the ohmic (Fig. 2c) and to a lesser extent the activation (Fig. 2d) losses participate towards the superiority of the conventional fuel cell over the air-breathing fuel cell in particular at high current densities (>500 mA/cm^2). The ohmic losses generally correlate to the cell temperature which has been set in this study to be that of the cathode catalyst layer; this is a reasonable arrangement as the temperature difference between the cathode catalyst layer (where temperature is a maximum) and the outermost sides of the fuel cells is, for a given current density, less than 2 °C. As the cell temperature increases, the water activity (calculated by Eq. (10)) decreases. To this end, the exponential increase in air-breathing fuel cell temperature after 500 mA/cm^2 causes a corresponding exponential increase in membrane resistance and in turn the ohmic losses. This exponential increase in air-breathing fuel cell temperature is attributed to the inability of the heat transfer coefficient (which is substantially lower than the corresponding forced convection heat transfer coefficient for the conventional fuel cell) to dissipate heat from the air-breathing fuel cell. As shown in Fig. 2e, the natural convection heat transfer coefficient increases with increasing current density; however, this increase is not sufficiently high to mitigate the exponential increase in cell temperature and, consequently, the ohmic losses.

Likewise, the exponential increase in the air-breathing fuel cell temperature causes a higher increased activation losses compared to the conventional fuel cell; this is evident from Eq. (3). This equation also shows that the activation losses are a function of oxygen concentration at the cathode catalyst layer: as the oxygen concentration increases, the activation losses decrease. In this regard, the conventional fuel cell has substantially higher amount of oxygen available for the reaction at the cathode catalyst layer than the air-breathing fuel cell (not shown) and this is due to significantly higher mass transfer coefficient demonstrated by the conventional fuel cell (Fig. 2f). It is noteworthy that both forced and natural mass transfer coefficient slightly increase with increasing current density as both are a function of diffusivity coefficient which scale with temperature as evidenced from Eq. (23) and Eq. (25).

In the following subsections, we conduct parametric studies to evaluate the effects of some key parameters (i.e., the GDL porosity, the GDL thickness, the membrane thickness and the electrical resistance) on the performance of both air-breathing and conventional fuel cells. This is performed in order to obtain insights on how the performance of air-breathing PEFC could be improved through analysing the differences in the outputs of the two types of the modelled fuel cells.

3.1. Porosity of gas diffusion layers

Fig. 3 shows the impact of the cathode GDL porosity on the performance of the modelled fuel cells. Interestingly, the performance of the air breathing PEFC improves with decreasing cathode GDL porosity while the conventional one shows a slight performance increase with increasing cathode GDL porosity (Fig. 3a). As expected, the increase in the cathode GDL porosity allows for more oxygen to be transported to the catalyst layers of the fuel cells (Fig. 3e). Equally, more water is removed from the cathode catalyst layer as the cathode GDL porosity increases (Fig. 3f). As heat transfer coefficient at the open cathode of the air-breathing PEFC is not sufficiently high to lower the exponential increase of the cell temperature (Fig. 3b), the amount of water needed to hydrate the polymer electrolyte membrane become a rate limiting factor. As the water concentration at the cathode catalyst layer (and the membrane electrolyte) of the air-breathing fuel cell decreases, the membrane resistance and subsequently the ohmic losses (Fig. 3c) increase, thus resulting in lower limiting current density (Fig. 3a).

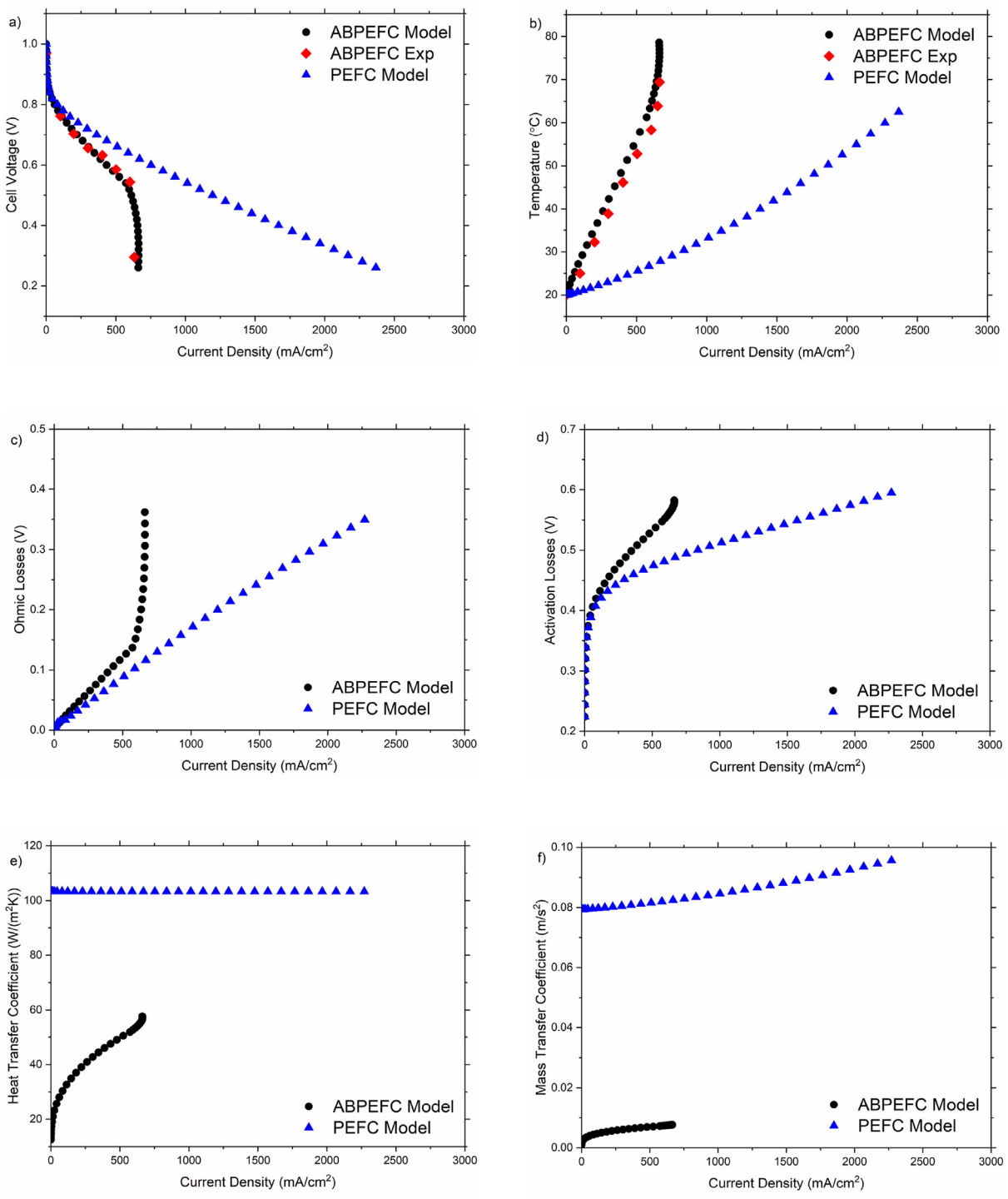

Fig. 2. The outputs of the modelled air-breathing and conventional PEFCs at 20 °C and 40% relative humidity: (a) cell voltage, (b) cell temperature, (c) ohmic losses, (d) activation losses, (e) heat transfer coefficient and (f) mass transfer coefficient of oxygen as a function of current density.

On the other hand, the heat transfer coefficients associated with the conventional fuel cell are sufficiently high to dissipate heat from the fuel cell and maintain well membrane hydration. As the porosity of the cathode GDL of the conventional fuel cell increases, more oxygen is transported to the cathode catalyst layer, thus leading to less activation losses (Fig. 3d) and better fuel cell performance (Fig. 3a).

The impact of anode GDL porosity on the performance of the modelled fuel cells are similar to but less than that of the cathode GDL porosity; see Fig. 4. Namely, as the anode GDL porosity of the

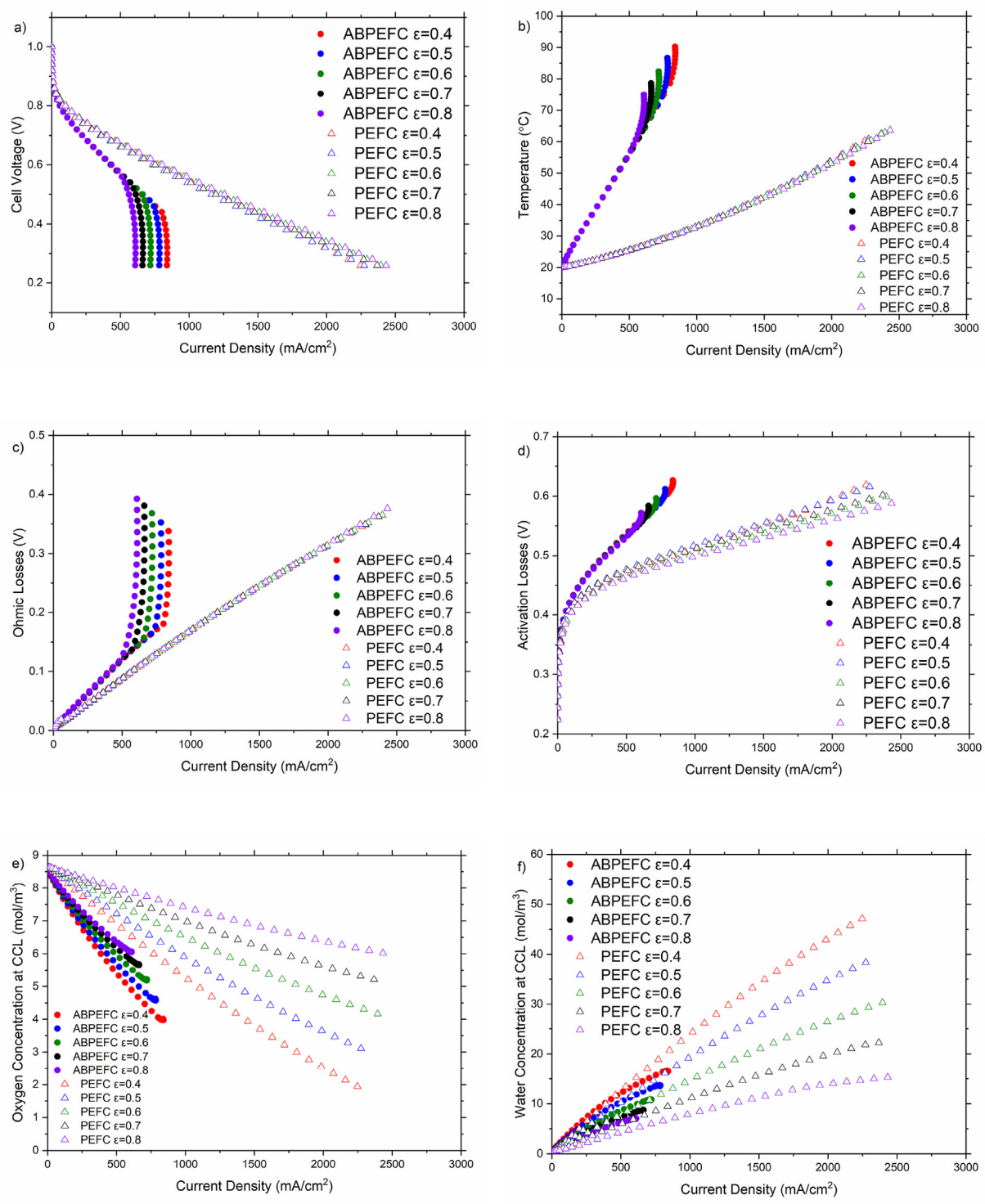

Fig. 3. The outputs of the modelled air-breathing and conventional PEFCs at 20 °C and 40% relative humidity and variable cathode GDL porosity: (a) cell voltage, (b) cell temperature, (c) ohmic losses, (d) activation losses, (e) oxygen concentration at the cathode catalyst layer and (f) water concentration at the cathode catalyst layer as a function of current density.

air-breathing fuel cell increases, the amount of water being removed from the anode catalyst layer (Fig. 4f) and the ohmic losses (Fig. 4c) increase. However, such an increase in the ohmic losses is less than that when the cathode GDL porosity increases considering the fact that water is generated at the cathode catalyst layer. On the other hand, the modelled conventional fuel cell is not heat transfer-limited and the increase in the anode GDL porosity leads to an increase in hydrogen available for the reaction at the

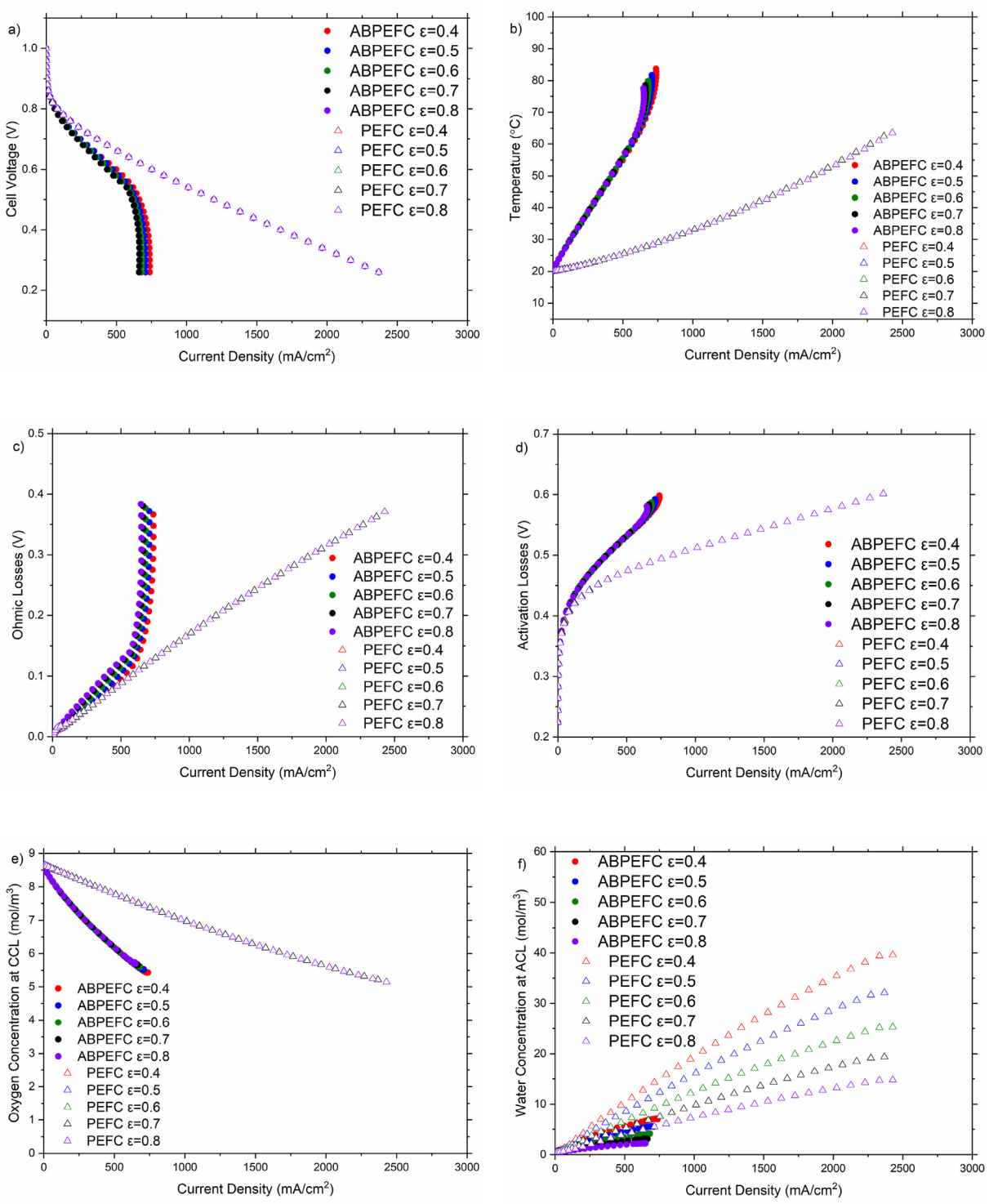

Fig. 4. The outputs of the modelled air-breathing and conventional PEFCs at 20 °C and 40% relative humidity and variable anode GDL porosity: (a) cell voltage, (b) cell temperature, (c) ohmic losses, (d) activation losses, (e) oxygen concentration at the cathode catalyst layer and (f) water concentration at the anode catalyst layer as a function of current density.

anode catalyst layer (not shown) and a very slight non-noticeable improvement in the fuel cell performance (Fig. 4a).

Overall, considering the outcomes of this study, it is recommended that GDLs with relatively low porosity (~0.4) should be used for air-breathing PEFCs, particularly for the cathode side of the fuel cell.

3.2. Thickness of gas diffusion layers

Fig. 5 and Fig. 6 show the impact of the thickness of the cathode GDL and the anode GDL respectively on the performance of the modelled fuel cells. It is clear that the impact of the GDL thickness is similar to that of the porosity. Namely, the performance of the air-breathing of the fuel cell improves as the cathode or anode GDL

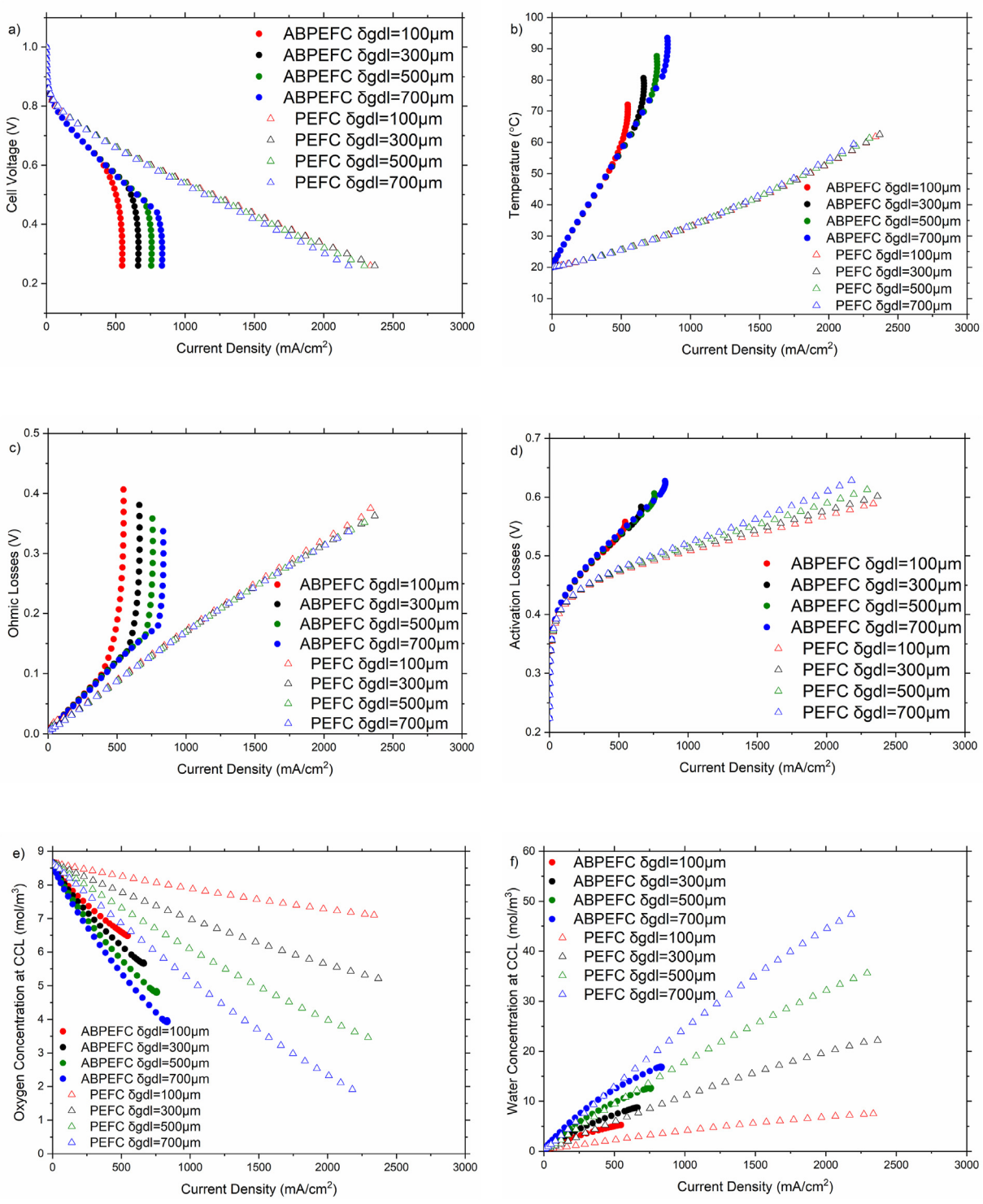

Fig. 5. The outputs of the modelled air-breathing and conventional PEFCs at 20 °C and 40% relative humidity and variable cathode GDL thickness: (a) cell voltage, (b) cell temperature, (c) ohmic losses, (d) activation losses, (e) oxygen concentration at the cathode catalyst layer and (f) water concentration at the cathode catalyst layer as a function of current density.

thickness increases (Figs. 5a and 6a). As the GDL thickness increases, less water is removed from the catalyst layers and the membrane (Figs. 5f and 6f), thus reducing the membrane resistance and subsequently the ohmic losses (Figs. 5c and 6c). On the other hand, the conventional fuel cell is not heat transfer limited due to high transfer coefficients that allow for reasonable cell temperatures compared to those of air-breathing fuel cells (Figs. 5b and 6b). To this end, thin GDLs are of benefits to the conventional fuel cell as it permits more oxygen to be supplied to the catalyst layers (Fig. 5e) and/or more heat to be dissipated from the fuel cell leading to less cell temperatures (Figs. 5b and 6b), less activation losses (Figs. 5d and 6d) and slightly better performance (Figs. 5a

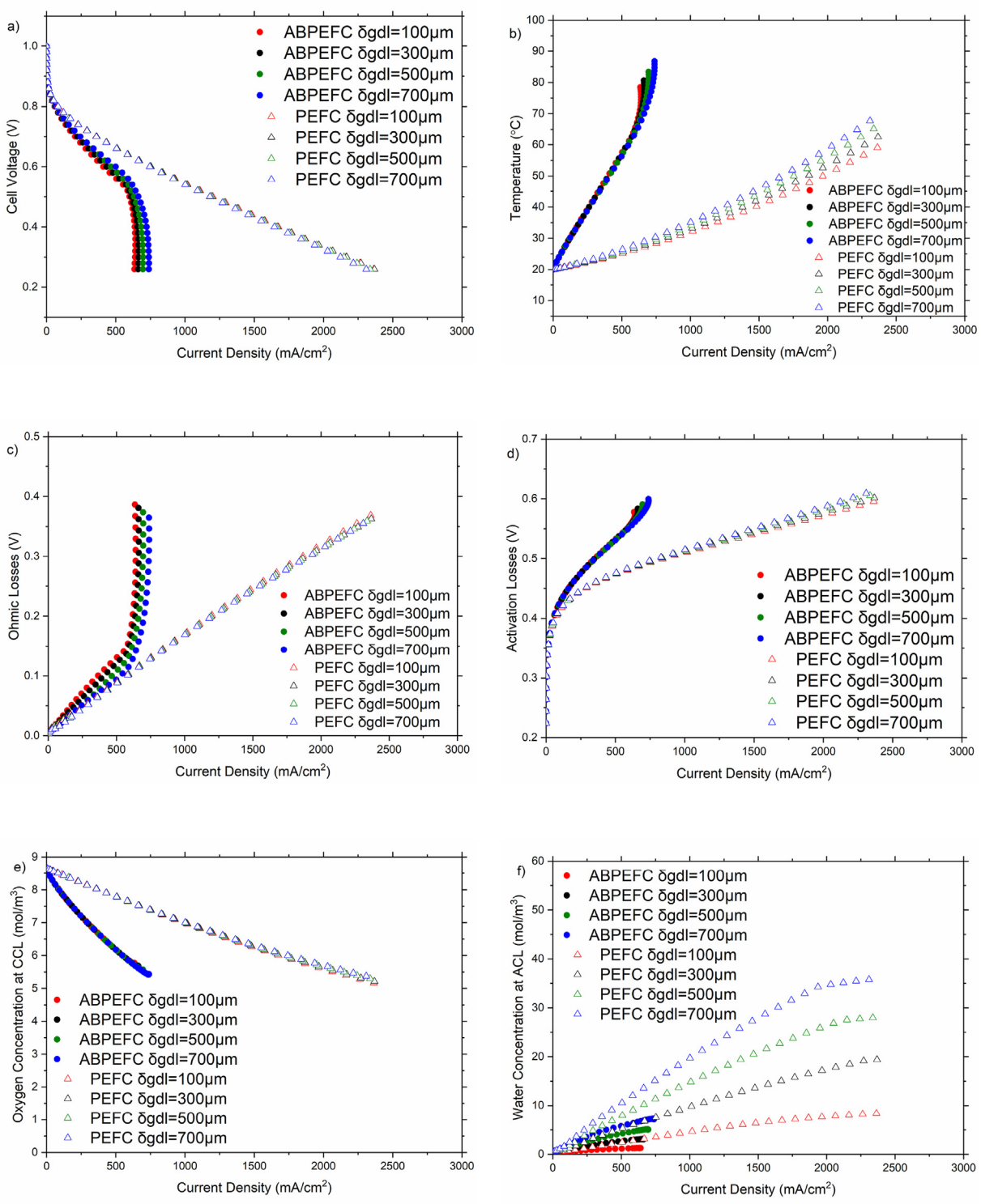

Fig. 6. The outputs of the modelled air-breathing and conventional PEFCs at 20 °C and 40% relative humidity and variable anode GDL thickness: (a) cell voltage, (b) cell temperature, (c) ohmic losses, (d) activation losses, (e) oxygen concentration at the cathode catalyst layer and (f) water concentration at the anode catalyst layer as a function of current density.

and 6a). It should be noted that, as with the impact of the GDL porosity, the impact of the cathode GDL thickness on the performance of either the air-breathing or the conventional fuel cell is more profound than that of the anode GDL thickness and this is due to two factors: (i) more water is available at the cathode catalyst layer where it is produced and (ii) activation losses are mainly associated with the cathode catalyst layer. One more observation is that the cell temperature of the conventional fuel cell is more sensitive to the thickness of the anode GDL than the cathode GDL. This could be attributed to the longer thermal pathway that heat generated at the cathode catalyst layer need to travel through to the surface of the anode GDL compared to the surface of the cathode

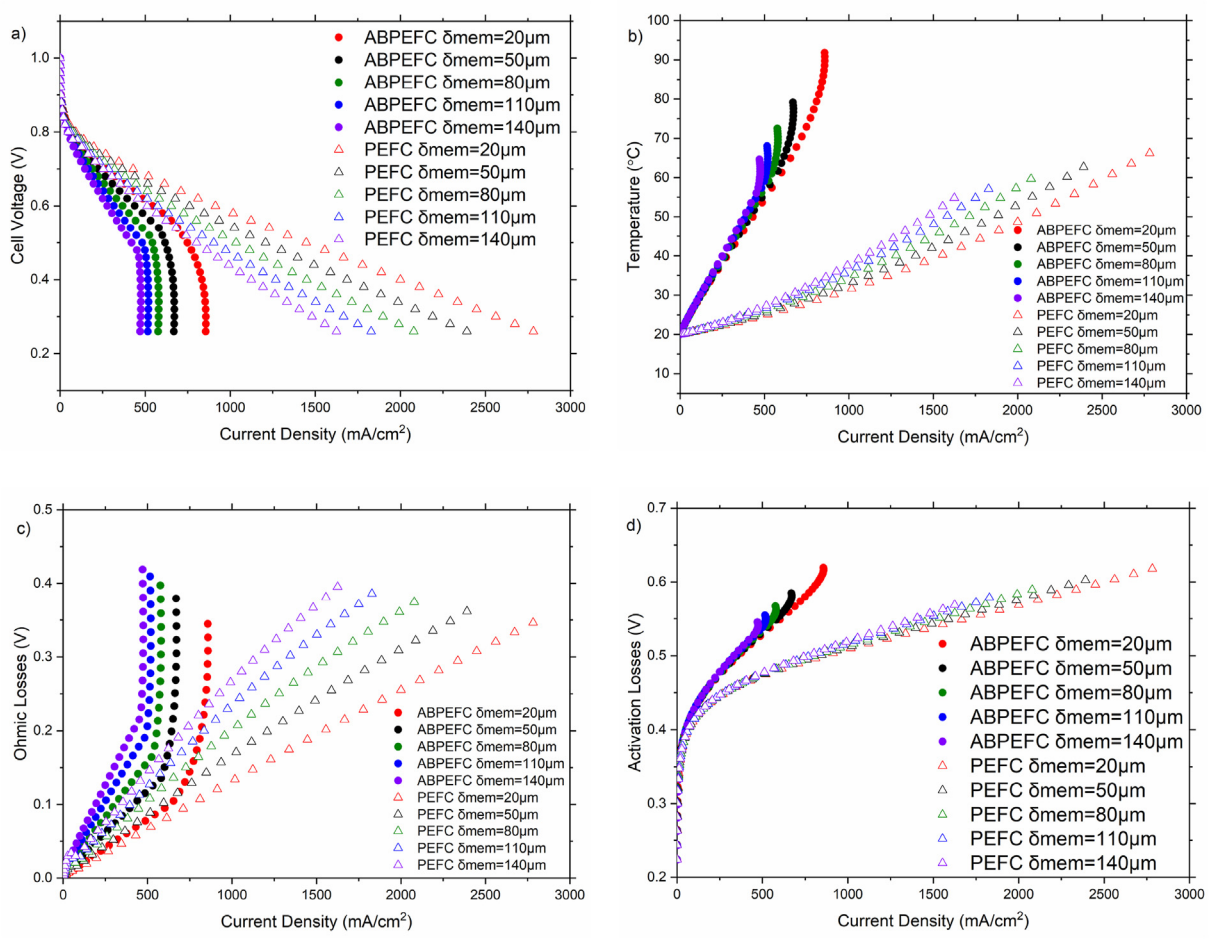

Fig. 7. The outputs of the modelled air-breathing and conventional PEFCs at 20 °C and 40% relative humidity and variable membrane thickness: (a) cell voltage, (b) cell temperature, (c) ohmic losses and (d) activation losses.

GDL; see Fig. 1. Therefore, any reduction in the anode GDL thickness will have greater (and better) impact on the surface temperature compared to that of the cathode GDL thickness. Overall, GDLs with relatively high thickness (>500 μm) are favoured to be used for air-breathing PEFCs, particularly for the cathode side of the fuel cell.

3.3. Membrane thickness

Fig. 7 shows the impact of the membrane thickness on the performance of the modelled fuel cells. For this parametric study, membrane thicknesses have been changed in equally-spaced intervals from 20 to 140 μm. Overall, the fuel cell performance degrades with increasing membrane thickness for either the air-breathing or the conventional fuel cell. Evidently, as the membrane thickness increases, the ionic resistance of the membrane and subsequently the ohmic losses increases (Fig. 7c). Also, the overall thermal resistance of the fuel cell increases with increasing membrane thickness, thus causing (along with increasing ohmic losses) an increase in cell temperature (Fig. 7b) and consequently activation losses (Fig. 7d). It is noteworthy that the fuel cell performance becomes less limited by the membrane thickness as the latter increases. For example, the limiting current density of the air-breathing fuel cell decreases by about 22% when changing the membrane thickness from 20 to 50 μm and by about 9% when changing the membrane thickness from 110 to 140 μm.

3.4. Electrical resistance

Fig. 8 shows the impact of the total electrical resistance on the performance of the modelled fuel cells. For the given range of the electrical resistance (6–18 *mΩ*), the performance of the air-breathing fuel cell in the intermediate current density region slightly degrades with increasing electrical resistance and ohmic losses (Fig. 8c); however, this effect diminishes as the current density increases as evidenced by the almost invariant limiting current densities of all the cases (Fig. 8a). The fuel cell resistance is, as could be seen from Eq. (5), broken down into electrical resistance and membrane (ionic) resistance. As the current density of the air-breathing fuel cell increases, more heat is generated due to increasing ohmic (Fig. 8c) and activation losses (Fig. 8d). The relatively poor heat dissipation from the air-breathing fuel cell results in an exponential increase of the cell temperature at high current densities which substantially lower the water activity and increase the membrane resistance (Fig. 8e) and eventually mask the impact of the electrical resistance. As can be seen from Fig. 8e, the values of the membrane resistance are almost the same at very high current

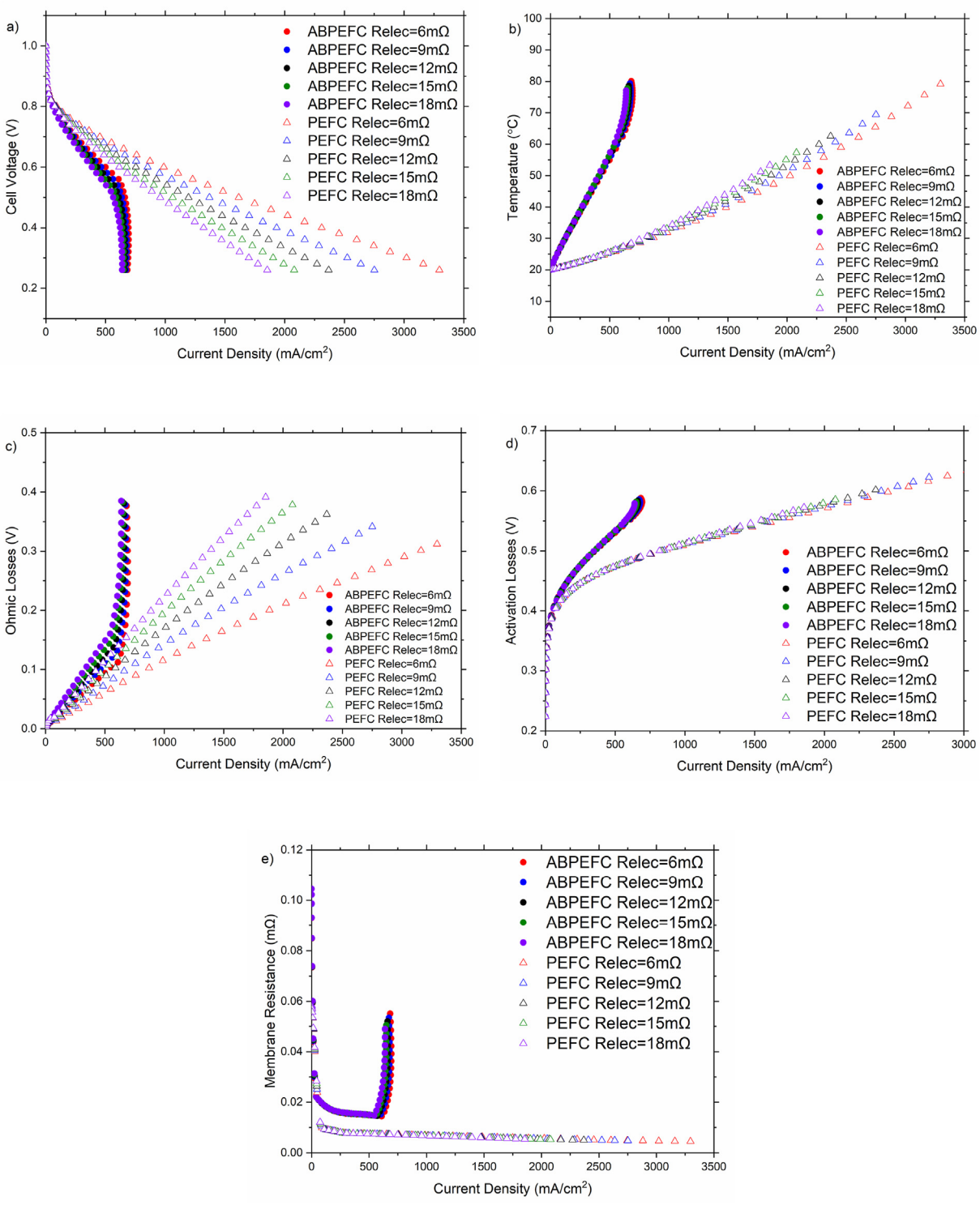

Fig. 8. The outputs of the modelled air-breathing and conventional PEFCs at 20 °C and 40% relative humidity and variable electrical resistance: (a) cell voltage, (b) cell temperature, (c) ohmic losses, (d) activation losses and (e) membrane resistance.

densities justifying the almost invariant current densities of all the investigated cases for the air-breathing fuel cell. On the other hand, the conventional fuel cell (compared to the air-breathing one) enjoys better heat dissipation which even allow the membrane conductivity to increase with linearly increasing cell temperature (see Eq. (8)). This in turn allows for the impact of the electrical resistance to be fully realised along the entire range of the current density of the conventional fuel cell: the fuel cell performance gradually degrades with increasing electrical resistance.

4. Conclusions

Two steady-state, non-isothermal mathematical models have been developed for air-breathing and conventional PEFCs in order

to undertake a parametric study that elucidates the key factors that influence the performance of each type of fuel cells and subsequently obtain better insights on how to improve the performance of the air-breathing fuel cell. Namely, some key parameters (i.e., the porosity and the thickness of the GDL, the membrane thickness and the overall electrical resistance) have been selected to comparatively assess the performance for each type of fuel cells and identify the underlying reasons behind the clear difference in performance. The key findings of this study are as follows:

- The conventional PEFC significantly outperforms the air-breathing PEFC and this is due to substantially higher heat and mass transfer coefficients demonstrated by the former type of fuel cells. Poor heat dissipation, due to reliance on natural heat convection, in case of the air-breathing PEFC leads to, compared to the conventional PEFC, an exponential increase in cell temperature at high current densities which ultimately lower the membrane hydration and increase the ohmic losses. Likewise, poor supply of oxygen to the cathode catalyst layer of the air-breathing PEFC results in increased activation losses.
- The porosity and the thickness of the GDL impact the performance of the air-breathing and conventional PEFCs differently. As the GDL porosity increases from 0.4 to 0.8 or the GDL thickness decreases from 700 to 100 μm in case of the air-breathing PEFC, the rate of water transport away from the catalyst layer (and the membrane) increases, lowering the hydration level of the membrane and consequently increasing the ohmic losses and degrading cell performance especially at high current densities where cell temperature increases exponentially. On the other hand, the conventional PEFC is not, owing to relatively high heat transfer coefficient, heat transfer limited and therefore the increase in the GDL porosity or the decrease in the GDL thickness lead to better performance due to increased supply of oxygen/hydrogen to the catalyst layers without compromising the membrane hydration level.
- Both the air-breathing and conventional PEFCs perform better with the thinnest membrane (i.e. 20 μm) and this is evidently due to decreased membrane resistance and subsequently ohmic losses. However, the performance of the air-breathing PEFC is more sensitive to membrane thickness than the conventional PEFC and this is due to the fact that the former type of fuel cells is more heat transfer limited, meaning that thicker membranes result in higher thermal resistance and ultimately more pronounced impact on cell performance.
- In contrast, the performance of the conventional PEFC was found to be more sensitive to the overall electrical resistance than the air-breathing PEFC. The ohmic losses in the air-breathing PEFC are, owing to insufficient heat dissipation at high current densities, dominantly influenced by the membrane resistance which largely mask the impact of the electrical resistance.
- As a recommendation out of this study, GDLs with relatively low porosity (~0.4) and high thickness (>500 μm) should be ideally designed and/or used for air-breathing PEFCs, particularly for the cathode side of the fuel cell.

Authors statement

Fatma Calili-Cankir: Conceptualization, Methodology, Software, Formal analysis, Investigation, Validation, Writing – original draft, Writing – review & editing, Visualization.; Mohammed S. Ismail: Conceptualization, Methodology, Software, Formal analysis, Investigation, Validation, Writing – original draft, Writing – review & editing, Supervision.; Derek B. Ingham: Supervision, Writing – review & editing.; Kevin J. Hughes: Supervision, Writing – review & editing.; Lin Ma: Supervision, Writing – review & editing.; Mohamed Pourkashanian: Supervision, Writing – review & editing, Project administration.

Declaration of competing interest

The authors declare that they have no known competing financial interests or personal relationships that could have appeared to influence the work reported in this paper.

Acknowledgements

Fatma Calili thanks the Ministry of National Education at the Republic of Turkey for funding her PhD studentship at the University of Sheffield.

Nomenclature

Roman symbols

a	Water activity [–]
A_{act}	Active area of the fuel cell [m^2]
C	Molar Concentration [mol/ m^3]
D	Diffusion coefficient [m^2/s]
e	Emissivity [–]
E	Nernst Voltage [V]
E_a	Activation energy [J/mol]
F	Faraday's constant [C/mol]
g	Gravitational acceleration [m/s^2]
h	Heat transfer coefficient [$W/(m^2.K)$]
h_m	Mass transfer coefficient [m/s]
ΔH	Enthalpy change for the reaction [J/mol]
j	Current density [A/m^2]
j_0	Reference exchange current density [A/m^2]
k	Thermal conductivity [W/(m.K)]
L_{ch}	Characteristic length [m]
M	Molecular weight [kg/m^3]
n	Number of electrons [–]
n_d	Electro-osmotic drag coefficient [–]
N	Molar flux [$mol/(m^2.s)$]
P	Ambient pressure [atm]
P_{H2}	Partial pressure of hydrogen [atm]
P_{H_2O}	Partial pressure of water vapour [atm]
P_{sat}	Water vapour saturation pressure [atm]
P_{O_2}	Partial pressure of oxygen [atm]
q	Heat flux [W/m^2]
R	Universal Gas Constant [atm/(mol.K)]
R_{elec}	Lumped electrical cell resistance [Ω]
R_{mem}	Membrane resistance [Ω]
Ra	Rayleigh number [–]
RH	Relative humidity [%]
ΔS	Entropy change for the reaction [J/(mol.K)]
Sh	Sherwood number [–]
T	Absolute temperature [K]
V_{cell}	Cell voltage [V]
x	Mole fraction [–]

Greek symbols

α	Charge transfer coefficient [−]
β	Thermal expansion coefficient [K^{-1}]
γ	Volumetric expansion coefficient [K^{-1}]
δ	Thickness [m]
ε	Porosity [−]
η_{act}	Activation losses [V]
η_{ohmic}	Ohmic losses [V]
λ	Water content [−]
σ_{Bolt}	Stephan-Boltzmann constant [$W/(m^2\ K^4)$]
σ_{mem}	Ionic conductivity [S/m]

Abbreviations

ABPEFC	Air-breathing Polymer Electrolyte Fuel Cell
ACL	Anode Catalyst Layer
CCL	Cathode Catalyst Layer
GDL	Gas Diffusion Layer
MEA	Membrane Electrode Assembly
PEFC	Polymer Electrolyte Fuel Cell

References

[1] Karatayev M, Lisiakiewicz R, Gródek-Szostak Z, Kotulewicz-Wisińska K, Nizamova M. The promotion of renewable energy technologies in the former Soviet bloc: why, how, and with what prospects? Energy Rep 2021;7:6983–94. https://doi.org/10.1016/j.egyr.2021.10.068.

[2] Hekimoğlu G, Sarı A, Kar T, Keleş S, Kaygusuz K, Yıldırım N, Tyagi VV, Sharma RK, Saleh TA. Carbonized waste hazelnut wood-based shape-stable composite phase change materials for thermal management implementations. Int J Energy Res 2021;45(7):10271–84. https://doi.org/10.1002/er.6514.

[3] Sarı A, Saleh TA, Hekimoğlu G, Tyagi VV, Sharma RK. Microencapsulated heptadecane with calcium carbonate as thermal conductivity-enhanced phase change material for thermal energy storage. J Mol Liq 2021;328:115508. https://doi.org/10.1016/j.molliq.2021.115508.

[4] Daud WRW, Rosli RE, Majlan EH, Hamid SAA, Mohamed R, Husaini T. PEM fuel cell system control: a review. Renew Energy 2017;113:620–38. https://doi.org/10.1016/j.renene.2017.06.027.

[5] Moazeni F, Khazaei J. Electrochemical optimization and small-signal analysis of grid-connected polymer electrolyte membrane (PEM) fuel cells for renewable energy integration. Renew Energy 2020;155:848–61. https://doi.org/10.1016/j.renene.2020.03.165.

[6] Rosli MI, Borman DJ, Ingham DB, Ismail MS, Ma L, Pourkashanian M. Transparent PEM fuel cells for direct visualization experiments. J Fuel Cell Sci Technol 2010;7(6). https://doi.org/10.1115/1.4001353.

[7] Wilberforce T, Ijaodola O, Khatib FN, Ogungbemi EO, El Hassan Z, Thompson J, Olabi AG. Effect of humidification of reactive gases on the performance of a proton exchange membrane fuel cell. Sci Total Environ 2019;688:1016–35. https://doi.org/10.1016/j.scitotenv.2019.06.397.

[8] Cha D, Yang W, Kim Y. Performance improvement of self-humidifying PEM fuel cells using water injection at various start-up conditions. Energy 2019;183:514–24. https://doi.org/10.1016/j.energy.2019.06.154.

[9] Wilberforce T, Alaswad A, Palumbo A, Dassisti M, Olabi AG. Advances in stationary and portable fuel cell applications. Int J Hydrogen Energy 2016;41(37):16509–22. https://doi.org/10.1016/j.ijhydene.2016.02.057.

[10] Tohidi M, Mansouri SH, Amiri H. Effect of primary parameters on the performance of PEM fuel cell. Int J Hydrogen Energy 2010;35(17):9338–48. https://doi.org/10.1016/j.ijhydene.2010.03.112.

[11] Carcadea E, Varlam M, Ismail M, Ingham DB, Marinoiu A, Raceanu M, Jianu C, Patularu L, Ion-Ebrasu D. PEM fuel cell performance improvement through numerical optimization of the parameters of the porous layers. Int J Hydrogen Energy 2020;45(14):7968–80. https://doi.org/10.1016/j.ijhydene.2019.08.219.

[12] Turkmen AC, Celik C. The effect of different gas diffusion layer porosity on proton exchange membrane fuel cells. Fuel 2018;222:465–74. https://doi.org/10.1016/j.fuel.2018.02.058.

[13] Kahveci EE, Taymaz I. Assessment of single-serpentine PEM fuel cell model developed by computational fluid dynamics. Fuel 2018;217:51–8. https://doi.org/10.1016/j.fuel.2017.12.073.

[14] Carton JG, Lawlor V, Olabi AG, Hochenauer C, Zauner G. Water droplet accumulation and motion in PEM (Proton Exchange Membrane) fuel cell mini-channels. Energy 2012;39(1):63–73. https://doi.org/10.1016/j.energy.2011.10.023.

[15] Carton JG, Olabi AG. Three-dimensional proton exchange membrane fuel cell model: comparison of double channel and open pore cellular foam flow plates. Energy 2017;136:185–95. https://doi.org/10.1016/j.energy.2016.02.010.

[16] Dong P, Xie G, Ni M. Improved energy performance of a PEM fuel cell by introducing discontinuous S-shaped and crescent ribs into flowing channels. Energy 2021;222:119920. https://doi.org/10.1016/j.energy.2021.119920.

[17] Zhang Y, Pitchumani R. Numerical studies on an air-breathing proton exchange membrane (PEM) fuel cell. Int J Heat Mass Tran 2007;50(23–24):4698–712. https://doi.org/10.1016/j.ijheatmasstransfer.2007.03.044.

[18] Zhang Y, Mawardi A, Pitchumani R. Numerical studies on an air-breathing proton exchange membrane (PEM) fuel cell stack. J Power Sources 2007;173(1):264–76. https://doi.org/10.1016/j.jpowsour.2007.05.008.

[19] O'Hayre R, Fabian T, Litster S, Prinz FB, Santiago JG. Engineering model of a passive planar air breathing fuel cell cathode. J Power Sources 2007;167(1):118–29. https://doi.org/10.1016/j.jpowsour.2007.01.073.

[20] Litster S, Pharoah JG, McLean G, Djilali N. Computational analysis of heat and mass transfer in a micro-structured PEMFC cathode. J Power Sources 2006;156(2):334–44. https://doi.org/10.1016/j.jpowsour.2005.05.064.

[21] Calili F, Ismail MS, Ingham DB, Hughes KJ, Ma L, Pourkashanian M. A dynamic model of air-breathing polymer electrolyte fuel cell (PEFC): a parametric study. Int J Hydrogen Energy 2021;46(33):17343–57. https://doi.org/10.1016/j.ijhydene.2021.02.133.

[22] Rajani BPM, Kolar AK. A model for a vertical planar air breathing PEM fuel cell. J Power Sources 2007;164(1):210–21. https://doi.org/10.1016/j.jpowsour.2006.10.055.

[23] Chen Z, Ingham D, Ismail M, Ma L, Hughes KJ, Pourkashanian M. Effects of hydrogen relative humidity on the performance of an air-breathing PEM fuel cell: a numerical study. Int J Numer Methods Heat Fluid Flow 2019. https://doi.org/10.1108/HFF-11-2018-0674.

[24] Matamoros L, Brüggemann D. Concentration and ohmic losses in free-breathing PEMFC. J Power Sources 2007;173(1):367–74. https://doi.org/10.1016/j.jpowsour.2007.02.091.

[25] Ying W, Ke J, Lee WY, Yang TH, Kim CS. Effects of cathode channel configurations on the performance of an air-breathing PEMFC. Int J Hydrogen Energy 2005;30(12):1351–61. https://doi.org/10.1016/j.ijhydene.2005.04.009.

[26] Ying W, Sohn YJ, Lee WY, Ke J, Kim CS. Three-dimensional modeling and experimental investigation for an air-breathing polymer electrolyte membrane fuel cell (PEMFC). J Power Sources 2005;145(2):563–71. https://doi.org/10.1016/j.jpowsour.2005.01.083.

[27] Ying W, Yang TH, Lee WY, Ke J, Kim CS. Three-dimensional analysis for effect of channel configuration on the performance of a small air-breathing proton exchange membrane fuel cell (PEMFC). J Power Sources 2005;145(2):572–81. https://doi.org/10.1016/j.jpowsour.2005.02.066.

[28] Wang Y, Ouyang M. Three-dimensional heat and mass transfer analysis in an air-breathing proton exchange membrane fuel cell. J Power Sources 2007;164(2):721–9. https://doi.org/10.1016/j.jpowsour.2006.11.056.

[29] Hwang JJ. Species-electrochemical modeling of an air-breathing cathode of a planar fuel cell. J Electrochem Soc 2006;153(8):A1584. https://doi.org/10.1149/1.2209567.

[30] Schmitz A, Ziegler C, Schumacher JO, Tranitz M, Fontes E, Hebling C. Modelling approach for planar self-breathing PEMFC and comparison with experimental results. Fuel Cell 2004;4(4):358–64. https://doi.org/10.1002/fuce.200400034.

[31] Kumar PM, Kolar AK. Effect of cathode design on the performance of an air-breathing PEM fuel cell. Int J Hydrogen Energy 2010;35(2):671–81. https://doi.org/10.1016/j.ijhydene.2009.10.086.

[32] Henriques T, César B, Branco PC. Increasing the efficiency of a portable PEM fuel cell by altering the cathode channel geometry: a numerical and experimental study. Appl Energy 2010;87(4):1400–9. https://doi.org/10.1016/j.apenergy.2009.09.001.

[33] Ismail MS, Ingham DB, Hughes KJ, Ma L, Pourkashanian M. Thermal modelling of the cathode in air-breathing PEM fuel cells. Appl Energy 2013;111:529–37. https://doi.org/10.1016/j.apenergy.2013.05.007.

[34] Ismail MS, Ingham DB, Hughes KJ, Ma L, Pourkashanian M. An efficient mathematical model for air-breathing PEM fuel cells. Appl Energy 2014;135:490–503. https://doi.org/10.1016/j.apenergy.2014.08.113.

[35] Yan WM, Zeng MS, Yang TF, Chen CY, Amani M, Amani P. Performance improvement of air-breathing proton exchange membrane fuel cell stacks by thermal management. Int J Hydrogen Energy 2020;45(42):22324–39. https://doi.org/10.1016/j.ijhydene.2019.08.146.

[36] Lee N, Lee J, Lee SW, Jang SS, Ju H. Parametric study of passive air-cooled polymer electrolyte membrane fuel cell stacks. Int J Heat Mass Tran 2020;156:119886. https://doi.org/10.1016/j.ijheatmasstransfer.2020.119886.

[37] Al-Anazi A, Wilberforce T, Khatib FN, Vichare P, Olabi AG. Performance evaluation of an air breathing polymer electrolyte membrane (PEM) fuel cell in harsh environments–A case study under Saudi Arabia's ambient condition. Int J Hydrogen Energy 2021;46(45):23463–79. https://doi.org/10.1016/j.ijhydene.2020.10.258.

[38] Lee J, Gundu MH, Lee N, Lim K, Lee SW, Jang SS, Kim JY, Ju H. Innovative cathode flow-field design for passive air-cooled polymer electrolyte membrane (PEM) fuel cell stacks. Int J Hydrogen Energy 2020;45(20):11704–13. https://doi.org/10.1016/j.ijhydene.2019.07.128.

[39] Fabian T, Posner JD, O'Hayre R, Cha SW, Eaton JK, Prinz FB, Santiago JG. The role of ambient conditions on the performance of a planar, air-breathing hydrogen PEM fuel cell. J Power Sources 2006;161(1):168–82. https://doi.org/10.1016/j.jpowsour.2006.03.054.

[40] O'hayre R, Cha SW, Colella W, Prinz FB. Fuel cell fundamentals. John Wiley & Sons; 2016.

[41] Sone Y, Ekdunge P, Simonsson D. Proton conductivity of Nafion 117 as measured by a four-electrode AC impedance method. J Electrochem Soc 1996;143(4):1254. https://doi.org/10.1149/1.1836625.

[42] Springer TE, Zawodzinski TA, Gottesfeld S. Polymer electrolyte fuel cell model. J Electrochem Soc 1991;138(8):2334. https://doi.org/10.1149/1.2085971.
[43] Xing L, Shi W, Su H, Xu Q, Das PK, Mao B, Scott K. Membrane electrode assemblies for PEM fuel cells: a review of functional graded design and optimization. Energy 2019;177:445–64. https://doi.org/10.1016/j.energy.2019.04.084.
[44] Atyabi SA, Afshari E, Wongwises S, Yan WM, Hadjadj A, Shadloo MS. Effects of assembly pressure on PEM fuel cell performance by taking into accounts electrical and thermal contact resistances. Energy 2019;179:490–501. https://doi.org/10.1016/j.energy.2019.05.031.
[45] Miao D, Chen W, Zhao W, Demsas T. Parameter estimation of PEM fuel cells employing the hybrid grey wolf optimization method. Energy 2020;193:116616. https://doi.org/10.1016/j.energy.2019.116616.
[46] Bergman TL, Incropera FP, DeWitt DP, Lavine AS. Fundamentals of heat and mass transfer. John Wiley & Sons; 2011.
[47] Ghiaasiaan SM. Convective heat and mass transfer. CRC Press; 2018.
[48] Mench MM. Fuel cell engines. John Wiley & Sons; 2008.
[49] Unsworth G, Dong L, Li X. Improved experimental method for measuring gas diffusivity through thin porous media. AIChE J 2013;59(4):1409–19. https://doi.org/10.1002/aic.13911.
[50] Jiao K, Li X. Water transport in polymer electrolyte membrane fuel cells. Prog Energy Combust Sci 2011;37(3):221–91. https://doi.org/10.1016/j.pecs.2010.06.002.